103359
#1

Submitted to *Smart Materials and Structures. 2007*

# Thermo-Mechanical Behavior of Epoxy Shape Memory Polymer Foams

*Matthew A. Di Prima* and Martha Lesniewski*
*School of Materials Science and Engineering, Georgia Institute of Technology*

*Ken Gall and David McDowelll*
*School of Materials Science and Engineering, Georgia Institute of Technology*
*George Woodruff School of Mechanical Engineering, Georgia Institute of Technology*

*Dr. Terry Sanderson*
*Raytheon Missile Systems*

*Douglas Campbell*
*Composite Technology Development*

**Abstract:**

*Shape memory polymer foams have significant potential in both bio-medical and aerospace fields, but there is relatively little understanding of their thermomechanical behavior under relevant deformation conditions. In this paper we examine the thermo-mechanical behavior of epoxy shape memory polymer foams with an average relative density of xx% deformed under conditions of varying stress, strain, and temperature. The glass transition temperature of the foams was measured to be approximately 90°C and compression and tensile tests were performed at temperatures ranging from 25 °C to 125 °C. Various shape recovery tests were used to measure recovery properties under different thermomechanical conditions. Tensile strain to failure tests as a function of temperature were used to probes the maximum recovery limits of the foam in both temperature and strain space. Compression tests were performed to examine compressibility of the material as a function of temperature; the present foams can be compacted as much as 90% and still experience full strain recovery over multiple cycles. Furthermore, both tensile strain to failure tests, and cyclic compression recovery tests, revealed that deforming at a temperature of 80°C minimizes micro-structural damage and maximizes macroscopic strain recovery. Deformation temperatures above or below this optimal value lead to lower failure strains in tension and the accumulation of non-recoverable strains in cyclic compression. Micro computed tomography scans of the foams at various compressed states were used to understand foam deformation mechanisms. The microCT studies revealed bending, buckling, and collapse of the cells with increasing compression, consistent with results from published numerical simulations.*

**Key words:** shape memory polymer, foam, microCT

*Correspondence: Email: matthew.diprima@gatech.edu; Telephone: (404)-385-0624

## 1. Introduction:

Shape memory polymer (SMP) foams possess a unique blend of low density, high compressibility, and shape memory properties that give them a wide range of potential applications. The majority of proposed applications are in the aerospace field [1-5] where the low density of the foam offsets relatively lower mechanical properties compared to solid shape memory polymers. Specific applications include space deployable support structures, shelters for space habitation, and rover components; a more exhaustive list can be found in W.M. Sokolowski et al [5]. The increased surface area of the foams has promise in biomedical implants [6] as embolic sponges. Before the potential of shape memory polymer foams can be reached, work must be performed to characterize complex thermo-mechanical response of the foams, and develop link between foam structure and thermo-mechanical properties.

SMP polymers have the ability to store and recover large strains. In thermally activated cross linked polymers, the shape memory effect is entropy driven. When heated above the glass transition temperature ($T_g$) the polymer chains can undergo rotational conformational changes, allowing the polymer chains to be uniaxially strained. As the material is strained, the alignment of the chains increases, which increases the stored energy in the material as the entropy of the chain decreases. This energy is subsequently locked into the polymer chains when the material is cooled below $T_g$ and the chains are restricted from freely rotating by interactions with their neighbors. When the polymer is reheated above $T_g$, without constraint, the entropy provides the driving force for the material to recover its initial shape [7]. The thermo-mechanical shape storage and recovery process is illustrated in Figure 1.

As the shape memory mechanism is relatively well understood, other aspects of the material have also been studied. These works can be arbitrarily divided into work on 'pure' SMPs [8-13] and work on SMP composites [14-18]. Work on 'pure' SMP is widespread. Shape memory polymer thin films have been studied and it was found that altering the materials $T_g$ shifted the mechanical properties in relationship to the new $T_g$ [8]. Research to develop constitutive models of the thermo-mechanical behavior has led to both 2D [9] and 3D models [10]. Thermal characterization and processing effects on material behavior have been performed

[11-13] and potential applications for SMPs were explored. Thermo-mechanical investigations similar to those performed in this work have been investigated in the 'pure' SMPs [8-10].

In order to increase the stiffness and recoverable force levels in shape memory polymers, various researchers have developed shape memory polymer based composites [14, 15]. Investigated SMP composites span fiber-reinforced materials [14, 15, 17] and nano-particulate SiC reinforced materials [16, 18]. As the percent of reinforcement increases, the modulus and recoverable force increases while the ductility and recoverable strain decreases [17]. This tradeoff in properties facilitates tailoring of a shape memory polymer for specific application requirement.

Foaming the SMP is another means to tailor material properties for application requirements. Foams generally have reduced mechanical stiffness and strength but enhanced compressibility and unique relationship between axial and transverse strains (Poissons effect). In general, foams can be classified into three different types; open celled where the cells are interconnected, closed cell where the cells are non-connecting, and a combination of open/closed cell [19]. This distinction allows for a greater understanding of mechanical properties and more accurate modeling of foam materials. Foams with open cells have been widely considered, and their internal structure and deformation mechanisms have been well characterized [20-23]. Other work has explored the effects of cell size distribution on modeling open cell foams [24-26]. Work on closed cell foams has also focused on determining/modeling the collapse behavior of these foams [27-31]. Under compression, nearly all foams exhibit similar regions in the stress strain curve, as presented in Figure 2: in he initial elastic regime and during early yield, struts deform uniaxially or bend, following this, the struts buckle as the material experiences plastic flow, and finally cells collapse and compact as strain is further increased and the stress-strain curve turns up toward higher stress at large strain [26, 31]. MicroCT scanning has been used to assist micro-structural analysis by allowing 3D imaging with micron range resolution to be generated from the foam [32]. The results can then be used to create FE models incorporating a realistic foam micro-structure [33].

Work to date on metallic and traditional polymer (elastomer) foams is much more complete than what has been accomplished on SMP foams. The bulk of literature on SMP foams has covered open celled polyurethane systems produced by Mitsubishi Heavy Industries [1-6]. The majority of this work concentrated on the long-term stability of foam 'frozen' in the deformed state, and it was observed that even after six months the deformed foam could fully recover the imposed deformation [3-5]. Other tests considered constrained stress and free strain recovery, cyclic properties, and strain rate dependence. These results demonstrated that full unconstrained recovery is possible from large compressive strains and that any external stress constraint inhibited full recovery but allowed for the foam to perform mechanical work [1-4]. Furthermore, there was no residual strain after cyclic compression when heated above $T_g$ [1, 3] and the effect of strain rate on mechanical properties increases when the foam is heated above the $T_g$ [2].

Although prior efforts have considered shape memory polymer foams, they have not studied a comprehensive suite of key thermo-mechanical deformation paths. Furthermore, prior studies on shape memory polymer foams provide minimal characterization of initial foam structure and no assessment of foam structure during storage and recovery paths. The purpose of this study is to provide a more thorough understanding of the thermo-mechanical storage and recovery behavior in thermoset shape memory foams under relevant deformation conditions. Moreover, the combination of macroscopic thermo-mechanical tests and x-ray micro computed tomography are used to help understand the fundamental link between pore structure and deformation regimes and recoverable strain limits. The microCT allows direct tracking of the foam structure during storage and recovery tests. Results from the present study are compared to prior work on polyurethane SMP foams, and ramification of the results on emerging applications of shape memory polymer foams are discussed.

## 2. Experimental Method

*Materials and Specimen*

The material used in this work was an epoxy foam with the trade name TEMBO® 3XE provided by Composite Technology Development (CTD). The exact chemistry and processing of the material is proprietary, although the material is a two-part thermoset epoxy network. The foam has a mean cell diameter is 0.472 mm, determined by microCT scans, and a density of 0.2 g/cc, resulting in a relative density of XX. For DMA samples, the material was rough cut then sanded to rectangular prisms 10 by 6 by 2 mm. The compression test samples were rough cut to rectangular prisms 17 by 17 by 20 mm and then punched into cylinders with diameters of 13.5 mm and heights of 20 mm. The cylinders were then thermally cycled above the $T_g$ to remove any strain from the sample preparation. Tensile specimens, 0.5 scaled ASTM D 638-03 Type IV dog bones, were laser cut from sheet of foam 2 to 3 mm thick. The ends of the dog bones were wrapped in aluminum foil to prevent slippage and failure in the grip region. Since the tensile samples were a bit small to constitute a representative material volume, given average pore diameter, multiple duplicate tests were conducted in tension to assure repeatability of results.

*Experimental Apparatus*

To determine the $T_g$, a Thermal Analysis DMA Q800 was used with tension clamps. The remainder of the tests were performed with a MTS Insight 2 uni-axial mechanical test frame with an attached thermal chamber. A thermocouple was located inside the thermal chamber and was placed adjacent to the sample. Negligible differences between machine cross-head and laser extensometer displacement measurements in compression led to the displacement being measured by the cross-head. High load capacity stainless steel platens were used to compress the foam cylinders. High load capacity tensile grips and a MTS LX300 laser extensometer were used for the tensile tests.

*Experimental Procedure:*

Six types of tests were performed for bulk properties: DMA, compression, block compression, tensile, cyclic loading, and shape memory. The shape memory tests composed of free strain and constrained shape recovery.

## DYNAMIC MECHANICAL ANALYSIS (DMA)

The foam specimen was wrapped with aluminum foil at the ends to avoid fracture occurring in the grips. With the use of a torque wrench, the upper clamp was tightened to 1 inch-pound of torque and the lower clamp was tightened to 2 inch-pounds of torque. The sample equilibrated at 25°C for two minutes and was then heated to 150°C at a rate of 5°C/min. The test was run under strain control; with a strain of 0.1%, a preload of 0.01 N, a force track rating of 150%, and a frequency of 1 hz.

## COMPRESSION TEST

The tests were conducted at five different temperatures; 25°C, 50°C, 75°C, 100°C, and 125°C. To insure uniform heating, the thermal chamber and each specimen was held at temperature for ten minutes for each temperature. To insure full contact of the platen on the sample, a pre-load of .2N was used. The cross-head as ramped at a rate of 3mm/min for a strain rate of 0.0025 $s^{-1}$. The sample was compressed to a load of 1950 N, nearly the maximum load for the test frame, and unloaded at the same rate until the minimum pre-load was again reached. Three specimens were run at each temperature to insure repeatability of trends.

## BLOCK COMPRESSION TEST

In this test the specimen was loaded to the first strain point, unloaded until the pre-load is reached, re-loaded to the second strain point, and so on until the load limit is hit in lieu of the eighth strain point and was run at five different temperatures: 25°C, 50°C, 75°C, 100°C, and 125°C. The strain end points for each temperature were determined by taking the maximum strain from the compression test and breaking it into eight equal segments. To insure uniform heating, the thermal chamber and each specimen was held at temperature for ten minutes for each temperature. To maximize resolution and test range, a 2kN load cell was used for the 25°C, 50°C, and 75°C tests and a 100 N load cell was used for the 100°C and 125°C tests. The load limit for the 2kN load cell was set to 1950 N and the 100N load cell was set to 95 N to prevent damage to the load cells. To insure full contact of the platen on the sample, a pre-load of 0.2N (2kN load cell) or 0.075N (100N load cell) was used. The cross-head moved at a rate of

3mm/min for a strain rate of 0.0025 $s^{-1}$. Three specimens were run at each sample to insure repeatability of trends.

TENSILE TEST

In this test, the specimen was loaded using MTS 2kN tensile grips with a crosshead rate of 1.00 mm/min, strain rate of 0.0025 $s^{-1}$, until mechanical failure. After wrapping the ends in aluminum foil and measuring the width and thickness of the gauge length, a piece of laser tape was placed on both ends of the nominal gage section of the dog bone. The nominal gage length, used for calculations of strain, was measured prior to and during testing with the laser extensometer. The sample was placed in the tensile grips so that the laser tape was facing the thermal chamber door, and the thermal chamber heated to the appropriate temperature. Several specimens were tested at 25°C, 50°C, 65°C, 70°C, 75°C, 80°C, 85°C, 90°C, 95°C, 100°C, 125°C, and 150°C. To insure uniform heating, the thermal chamber and each specimen was held at temperature for ten minutes for each temperature. Once the specimen was at temperature, the load cell was zeroed and the testing began.

CYCLIC LOADING TEST

In this test each specimen was compressed in the load frame to a set strain endpoint for one hundred cycles. The standard cylindrical sample geometry was used with a cross-head rate of 3mm/min for a strain rate of $0.0025^{-1}$ s. The temperatures of interest for this test were 80°C, 100°C, and 125°C and the strain end points were 40%, 60%, and 80% engineering strain. To insure uniform heating, the thermal chamber and each specimen was held at temperature for ten minutes. For the tests at 80°C, the sample was heated to 100°C for recovery and cooled back to 80°C since at this testing temperature instantaneous (rubbery) recovery is not observed. With this extra step, the tests at 80°C were only cycled twenty times in light of excessive testing time. For the best resolution, a 100 N load cell was used with a load limit of 95 N (the load limit was set but not used). To insure full contact of the platen on the specimen, a pre-load of 0.075N was used.

SHAPE STORAGE

Shape storage is the first step for both constrained recovery and free strain recovery. The specimen was heated to the packaging temperature and compressed to a strain of 80%. This compression was maintained as the specimen was cooled to 25°C and the platen was raised when there was no longer a stress registering on the load cell. For this work, packaging temperatures of 100°C and 125°C were used.

## CONSTRAINED RECOVERY

The packaged specimen was placed into the MTS Insight 2 mechanical test frame with a 100N load cell and attached thermal chamber and compressed at room temperature to a pre-load of 0.5N. The compression platen was then raised 0.3 mm to take into account thermal expansion. The platen was then held at that position as the temperature was increased from 25°C to 145°C at 2°C/min. The stress exerted by the specimen on the platen was then recorded versus time, which was correlated to the temperature.

## FREE STRAIN RECOVERY

A cut down glass slide, with laser tape on one edge, was set on top of the packaged specimen. The specimen was then placed on a single compression platen, also with laser tape on the edge, in the MTS Insight 2 with attached thermal chamber. Three aluminum blocks were used to prevent the sample from falling over during the recovery process. The specimen was then heated from 25°C to 145°C at 2°C/min while the MTS LX300 laser extensometer recorded the displacement of the two pieces of laser tape. This displacement was used to determine to percent strain recovered and plotted against the temperature (again correlated through time).

## X-RAY MICRO-CT SCANNING

Various samples of interest were scanned using a Scanco Medical vivaCT 40 x-ray micro-CT scanner. A scan series of particular interest was the 125°C iterative scan and compression. In this series, a single sample was scanned and then compressed to 10% strain. That sample was then rescanned and compressed another 10% strain of original height until the sample was compressed to a strain of 80% the original height. Isolation of the same foam region across the scans was performed visually using ImageJ software for comparison and image

alignment. The MRIcro program was used for fine tuning area selection and generation of the 3D images. The average cell size for each scan was determined using ScanCo analysis software.

**3. Results**

A selected pair of storage modulus and tan delta from the DMA test are shown in Figure 3 and the differences between the resin and foam versions of the base material are readily visible. The $T_g$ of the foam is seen to be 92°C +/- what?? Do you have duplicates?, using the peak of the tan delta, with the onset near 75°C and the completion near 110°C. Figure 4 contains the result of this testing of a) simple compression and b) block compression. From 4a, it is seen that as the temperature increases so does the strain needed to fully compress the material. The curves from 4a and 4b overlay nicely, indicating that the block compression testing does not alter the mechanical properties in relation to the simple compression test. Figure 4c compares the low strain regions of the five temperatures, the log scales reveals the magnitude in the shift of the mechanical properties at small strains between the temperatures.

Figure 5a illustrates the loading path for the block compression test and the definition of the maximum strain ($e_M$) and recovered strain ($e_R$). 5b shows the effect of the maximum strain and the testing temperature on the materials ability to recover strain. At temperatures below $T_g$ the only strain recovered is elastic strain (roughly constant), so the ratio of $e_M$ to $e_R$ decreases as the maximum strain increases. The influence of $T_g$ on spontaneous shape recovery (rubbery behavior) is very visible in the difference of the plot of the samples run at 100°C versus the samples run at 75°C.

The results of the tensile testing versus temperature are presented in Figure 6. Figure 6a plots the tensile strain to failure versus temperature and compares it to the storage modulus measure through DMA testing. The error bars mark one standard deviation from the mean strain to failure for n = 3. Figure 6b is an overlay of selected tensile curves for each temperature which forms the failure peak [34]. These plots show that the optimum temperature to maximize tensile strain is approximately 80°C which is below $T_g$ measured by DMA

The results from the cyclic loading series (brought to 100 cycles) are contained in Figure 7. Figure 7a has selected cycle curves and defines the stress nomenclature at the strain end point. Figure 7b and 7c show the maximum stress achieved at the strain end point versus cycle number. The stress is normalized to the stress at the strain end point for the first cycle to allow comparison across temperature and strain end points. The trend is for there to be a sharp drop in the first few cycles and then for the normalized stress to plateau. Figure 8 compares the unrecovered strain from the cycling for the first 20 cycles to allow comparisons of the cyclic series at 80°C (which was only run to 20 cycles due to excessive testing time incurred during intermittent reheating to 100 °C). Figure 8a compares the samples compressed to 40%, Figure 8b compares the samples compressed to 60%, and Figure 8c compares the samples compressed to 80%. The temperature and maximum strain level has a significant effect on reversibility (accumulation of permanent strain) in the temperature range near Tg and close to the maximum strain capacity of the material. It is important to notice the difference in the scales of Figures 8a-8c.

The constrained recovery tests show that the specimen packaged at 100°C begins exerting stress at a slightly lower temperature than when the specimen is packaged at 125°C, as shown in Figure 9a. Furthermore, the foam packaged at 100°C exerts a greater force than when the foam is packaged at 125°C. The results from the free strain recovery test, Figure 9b, demonstrates that the packaging temperature does not affect the overall recovery, only the onset temperature of strain recovery.

In a high resolution CT scan, the cells in the undeformed foam are highly spherical (Figure 10). Furthermore, the wall thickness is non-uniform across the cell to cell interface. While the high resolution (6 μm) scan captures more of the cell wall than the 20 μm scan in Figure 11b, the overall structure is the same. The response of the cell to deformation is tracked in Figure 11; cell response to strain (with the stress-strain curve for comparison) is plotted in (a), while (b) shows micro-structural snapshots at increasing strains. The average cell size drops less than 10 percent in the first 10 percent of strain but then rapidly decreases until ~45 percent strain. After this point the decrease in the average cell size begins to slow. The micro-structural snapshot shows that buckling of the main cells did not occur on average until the sample was

compressed to 20 percent strain and that densification started near 40 percent strain. Each of the snapshots shown at 2mm by 2 mm by 0.8 mm in volume. Figure 10c shows histograms of cell size (cell wall spacing) for selected strain levels, showing that the distribution of cells sizes changes along with the average cell size.

**4. Discussion**

The results here provide a foundation to understand the thermo-mechanical behavior of shape memory polymer foams for emerging applications. The epoxy-based foams considered here are most applicable in the aerospace field, but some of the overarching results can be extened to other foam systems, especially thermoset networks. The compressive monotonic stress-strain results provide key information on the stiffness and compressibility of the foams as a function of strain level and temperature. The compressive stress-strain response, as a function of temperature, also constitutes the major input needed for constitutive modeling of the shape memory polymer foams. The tensile monotonic results provide key information on the ductility of the foams and the optimal temperature for deforming the foams without damage (under tension or compression). The cyclic results extend durability concepts to multiple loading cycles and provide increased sensitivity to local damage through changes in the stress-strain response (maximum stress, elastic modulus) with cycling. From a basic science perspective the cyclic results reveal local damage evolution trends that may not be evident under monotonic loading. From an application point of view the cyclic results provide a more conservative temperature and strain limits for the polymers to avoid failure. The free strain recovery test provides insight into the effect of deformation temperature on required actuation temperature while the constrained stress recovery test quantifies actuation work output. Finally, the microCT scanning provides some insight into the deformation mechanisms operating during foam compaction, although further work is surely needed to understand local deformation mechanisms operating during cyclic deformation.

The results from Figure 3 were used to determine the relative testing temperatures for the thermo-mechanical testing. From this plot, the five temperatures of interest for the thermo-mechanical testing were chosen to be 25°C, 50°C, 75°C, 100°C, and 125°C and corresponds to room temperature, the glassy phase, the transition onset, the transition completion, and the

rubbery phase. This provides a map of the mechanical properties over the full range of possible temperatures that the material could see in a shape memory cycle. Compression tests at these various temperatures are critical for future constitutive modeling efforts.

Post recovery analysis with calipers has shown full to nearly full recovery in samples that are heated above $T_g$ to induce recovery. While Figures 5b and 9b show that a great deal of strain is recovered, they do not show the full recovery that is observed after the test. In the case of Figure 5b, the slight minimum preload from the compression platen (0.075N) is preventing complete recovery in the course of the test. This effect was observed when the 100 N load cell was used instead of the 2 kN as the strain recovered increased when the minimum load was dropped from 0.5 N to 0.075 N. These minimum loads were required to maintain contact between the compression platens and the specimen. Using a microscope slide as a marker for the free strain recovery tests (Figure 8b) should have eliminated the effect of a load on the shape recovery and in fact the test shows greater strain recovery than Figure 5b. However, the test still does not show the full strain recovery as observed when the specimen is removed from the thermal chamber and measured by hand. This slight offset in strain recovery is most likely due to thermal expansion of the specimen post-measurement and pre-compression. The specimen is being compressed based off of its 'cold' height, so any height gained from thermal expansion would reduce the compressive strain of the sample and can account for the 2.3% offset in Figure 9b.

Figure 5b, which leads to Figure 7b, confirms the significance of the temperature for strain recovery in this foam system. The clearest indication is the change in trends between temperature above $T_g$ and below $T_g$. An unexpected result was that at the highest temperature, 125°C, the strain recoverability repeatedly dropped after being compressed to 80% strain (Figure 5b). This suggests that this temperature and strain are beyond the optimum conditions for this material to recover strain. This is reinforced by the results of Figure 7; where the cyclic response of the material being compressed to 80% strain at 125°C strongly deviates from the other curves. There is, however, little difference between the curves for 40% and 60% strain indicating that the temperature increase alone (both above $T_g$) is not enough to degrade the materials performance. The general trend of these curves, except for the aforementioned 80% at 125°C, is supported by

the literature on the cyclic properties of SMP foams [1-3], although the polyurethane foams exhibited a smaller drop in normalized stress. However, these polyurethane foams were all open celled with relative densities under 10 percent so differences in behavior is to be expected.

The peak of in the tensile strain to failure versus temperature in Figure 6a was a surprising result. This peak is theorized for elastomeric materials [34] and has been ecently confirmed in other SMP systems **[reference?]** and is not an anomaly to this material system. We believe that this peak signifies that the effects of material and/or structural defects are minimized at the peak, 80°C, where the material has enough viscoelasticity to suppress local damage in the polymer. This prompted a return to cyclic testing to investigate whether packaging at this temperature led to an increase in performance. Figure 8 shows that cyclic loading at 80°C exhibits less damage (less permanent strain) than the other testing temperatures at all three strain levels. As such, the peak in the tensile strain to failure does predict the optimum packaging temperature of the material to minimize damage during cyclic loading and unloading. It is interesting that this toughening mechanism is available to shape memory polymers, but not transitional elastomers since the latter materials are required to exhibit spontaneous strain recovery rather than strain recovery upon reheating.

The shape recovery tests, especially constrained stress recovery, show a dependency on the packaging temperature. In Figure 9a there is a noticeable difference in the stress-temperature curve between the specimen packaged at 100°C and 125°C. At 100°C the material is still in the visco-elastic region, as seen from the DMA data in Figure 3, which can account for the increase in constrained stress. The packaging temperature, as previously mentioned, affects the strain recovery onset and offset in the free strain recovery test. From Figure 7b, the specimen packaged at 100°C has an early onset and later offset of shape recovery than the specimen packaged at 125°C. Like the differences in the constrained stress recovery, this difference is most likely due to the visco-elastic behavior stored in the specimen packaged at 100°C.

As previously discussed, foam materials have three stages of deformation; bending, buckling, and densification [26, 31]. The results from Figure 10 shows that the epoxy SMP foam deforms consistent with these prior numerical predictions. The initial small drop in cell size in

Figure 10a can be explained as the cells bending in response to the stress. The next stage of buckling describes the rapid drop in the average cell size over the strain range of 10 to ~45 percent strain. Once the cell walls have all buckled, densification occurs which has a slower rate of cell size change and is seen at the end of 9a. This is supported by the images in Figure 10b, in which the main cells buckle between the 20 percent strain scan the 30 percent strain scan. The cells become difficult to distinguish when densification started around the 50 percent strain scan. The work here is the first to confirm these numerical predictions with experimental measurements.

## 5. Conclusion

1. Epoxy shape memory foams are capable of recovery from compressive strains of up to 90% depending of the prescribed themomechanical cycles.
2. There is both a temperature and strain dependence on the strain recovery under monotonic loading. The threshold observed in this work was at 125°C and for strains beyond 80%, after which there is a sharp decrease in strain recoverability under monotonic loading.
3. Cyclic strain recovery results in damage to the foam. This damage can be greatly minimized by lowering the strain end point or changing deformation temperature. The effect of temperature on damage is similar to that seen in the monotonic testing.
4. Approximately 80°C is the optimum temperature to package the current material to minimize structural damage.
5. The packaging temperature does strongly affect the unconstrained shape recovery profile.
6. The microCT scans show that the cell structure does deforms as predicted in numerical models of foam deformation.

**Acknowledgements**

This work was funded by Raytheon Missile Systems and through the AFRL with Air Force Contract No. FA9550-06-C-0109. The authors also thank Angela Lin at the Georgia Institute of Technology Orthopaedic Bioengineering Laboratory for assistance with the Micro-CT scanning.

**Reference:**

1. A.M. Watt, S. P., W.M. Sokolowski "Thermomechanical Properties of a Shape Memory Polymer Foam." Smart Materials and Structure. Submitted, 2001.

2. H. Tobushi, K. O., M. Endo, S. Hayashi (2001). "Thermomechanical Properties of Polyurethane-Shape Memory Polymer Foam." Journal of Intelligent Material Systems and Structures **12**: 283-287.

3. H. Tobushi, R. M., S. Hayashi, D. Shimada (2004). "The influence of shape-holding conditions on shape recovery of polyurethane-shape memory polymer foams." Smart Materials and Structures **13**: 881-887.

4. S.J. Tey, W. M. H., W.M. Sokolowski (2001). "Influence of long-term storage in cold hibernation on strain recovery and recovery stress of polyurethane shape memory polymer foam." Smart Materials and Structures **10**: 321-325.

5. W.M. Sokolowski, A. B. C., S. Hayashi, T. Yamada (1999). Cold hibernated elastic memory (CHEM) self-deployable structures. SPIE International Symposium on Smart Structures and Materials, Newport Beach, CA.

6. A. Metcalfe, A. C. D., I. Salazkin, L. Yahia, W.M. Sokolowski, J. Raymond (2003). "Cold Hibernated elastic memory foams for endovascular interventions." Biomaterials **24**: 491-497.

7. A. Lendlein, S. K. (2002). "Shape-Memory Polymers." Angewandte Chemie International Edition **41**: 2034-2057.

8. H. Tobushi, H. H., E. Yamada, S. Hayashi (1996). "Thermomechanical properties in a thin film of shape polymer of polyurethane series." Smart Materials and Structure **5**: 483-491.

9. H. Tobushi, K. O., S. Hayashi, N. Ito (2001). "Thermomechanical constituitive model of shape memory polymer." Mechanics of Materials **33**: 545-544.

10. Y. Liu, K. G., M. Dunn, A. Greenberg, J. Diani (2006). "Thermomechanics of shape memory polymers: Uniaxial experiments and constituitive modeling." International Journal of Plasticity **22**: 279-313.

11. H.M. Jeong, S. Y. L., B.K. Kim (2000). "Shape memory polyurethane containing amorphous reversible phase." Journal of Materials Science **35**: 1579.

12. S. Hayashi, S. K., P. Kapadia, E. Ushioda (1995). "Room-Temperature-Functional Shape-Memory Polymers." Plastics Engineering **51**(2): 29-31.

13. S. Hayashi, Y. T., N. Hayashi, Y. Akita (2004). "Developement of Smart Polymer Materials and its Various Applications." Mitsubishi Heavy Industries, Ltd. Technical Review **41**(1): 1-3.

14. Abrahamson, E. R., M. S. Lake, et al. (2003). "Shape Memory Mechanics of an Elastic Memory Composite Resin." Journal of Intelligent Material Systems and Structures **14**(10): 623-632.

15. K. Gall, M. M., N.A. Munshi, F. Beavers, M. Tupper (2000). "Carbon Fiber Reinforced Shape Memory Polymer Composite." Journal of Materials Systems and Structures **11**: 877-886.

16. K. Gall, M. L. D., Y. Liu, D. Finch, M. Lake, N.A. Munshi (2000). "Shape memory polymer nanocomposites." Acta Materialia **50**: 5115-5126.

17. T. Ohki, Q. Q. N., N. Ohsako, M. Iwamoto (2004). "Mechanical and shape memory behavior of composites with shape memory polymer." Composites: Part A **35**: 1065-1073.

18. Y. Liu, K. G., M.L. Dunn, P. McCluskey (2004). "Thermomechanics of shape memory polymer nanocomposites." Mechanics of Materials **36**: 929-940.

19. ASTM D 6226-05, "Standard Test Method for Open Cell Content of Rigid Cellular Plastics." ASTM International.

20. J. Zhou, W. O. S. (2004). "Mechanics Modeling of the Compressive Stiffness and Strength of Open-Celled Aluminum Foams." Materials and Manufacturing Processes **19**(5): 863-882.

21. L. Gong, S. K. (2005). "Compressive response of open cell foams. Part II: Initiation and evolution of crushing." International Journal of Solids and Structures **42**: 1381-1399.

22. L. Gong, S. K., W.-Y. Jang (2005). "Compressive response of open-cell foams. Part I: Morphology and elastic properties." International Journal of Solids and Structures **42**: 1355-1379.

23. Y. Wang, G. G., A.M. Cuitiño (2000). "The Deformation Habits of Compressed Open-Cell Solid Foams." Journal of Engineering Materials and Technology **122**: 376-378.

24. A.P. Roberts, E. J. G. (2001). "Elastic Moduli of Model Random Three-Dimensional Closed-Cell Cellular Solids." Acta Materialia **49**: 189-197.

25. A.P. Roberts, E. J. G. (2002). "Elastic properties of model random three-dimensional open-cell solids." Journal of the Mechanics and Physics of Solids **50**(1): 33-55.

26. M.W. Schraad, F. H. H. (2006). "A stochastic constitutive model for disordered cellular materials: Finite-strain uni-axial compression." International Journal of Solids and Structures **43**: 3542-3568.

27. Onck, P. R. (2001). "Application of a continuum constitutive model to metallic foam DEN-specimens in compression." International Journal of Mechanical Sciences **43**: 2947-2959.

28. P.A. Du Bois, S. K., M. Koesters, T. Franks (2006). "Material behaviour of polymers under impact loading." International Journal of Impact Engineering **32**: 725-740.

29. S.L. Lopatnikov, B. A. G., J.W. Gillespie Jr. "Modeling the progressive collapse behavior of metal foams." International Journal of Impact Engineering **In Print**.

30. T.-J. Lim, B. S., D.L. McDowell (2002). "Behavior of a random hollow sphere metal foam." Acta Materialia **50**: 2867-2879.

31. W. Ehlers, B. M. (2003). "A macroscopic finite strain model for cellular polymers." International Journal of Plasticity **19**: 961-976.

32. M.D. Montminy, A. R. T., C.W. Macosko (2004). "The 3D structure of real polymer foams." Journal of Colloid and Interface Science **280**: 202-211.

33. S. Youssef, E. M., R. Gaertner (2005). "Finite element modelling of the actual structure of cellular materials determined by X-ray tomography." Acta Materialia **53**: 719-730.

34. T. Smith (1963). "Ultimate Tensile Properties of Elastomers. I. Characterization by a Time and Temperature Independent Failure Envelope." Journal of Polymer Science. Part A, **1**: 3597-36.

**Figure 1:**

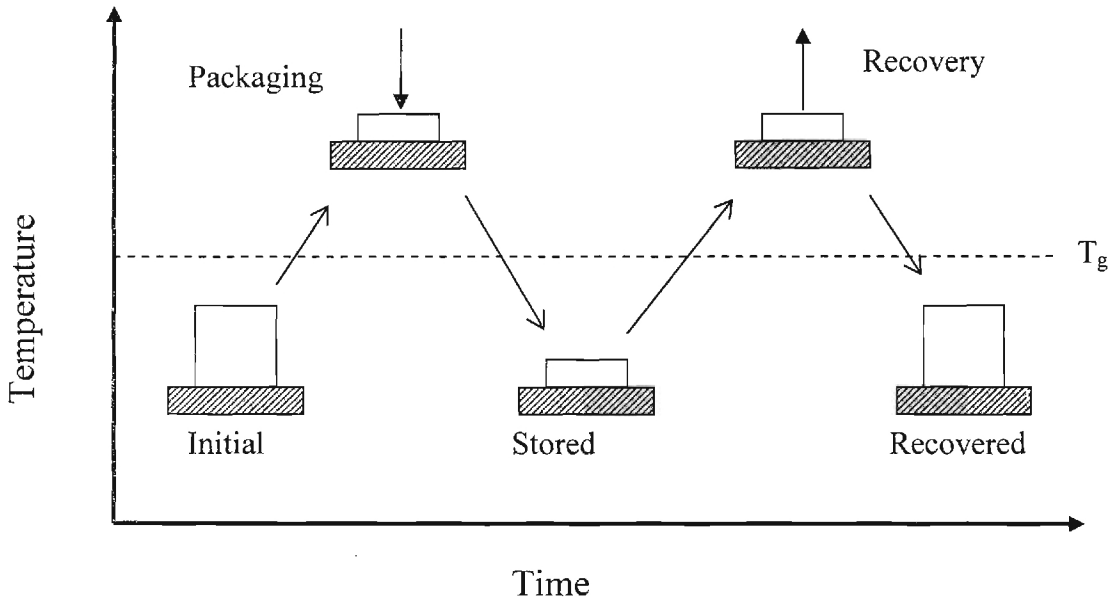
Packaging
Recovery
Temperature
$T_g$
Initial
Stored
Recovered
Time

**Figure 2:**

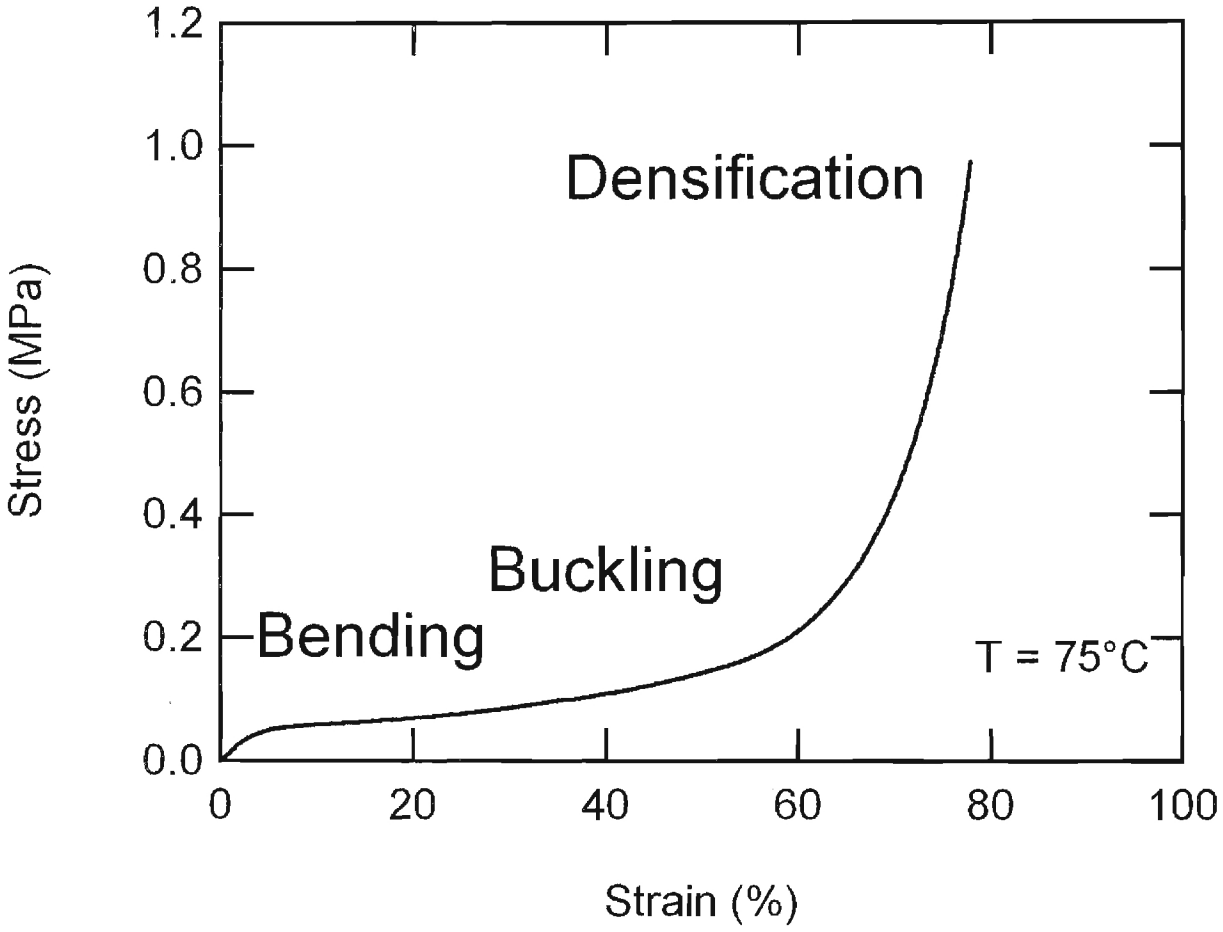
1.2
1.0
0.8
0.6
0.4
0.2
0.0
Stress (MPa)
Densification
Buckling
Bending
T = 75°C
0
20
40
60
80
100
Strain (%)

**Figure 3:**

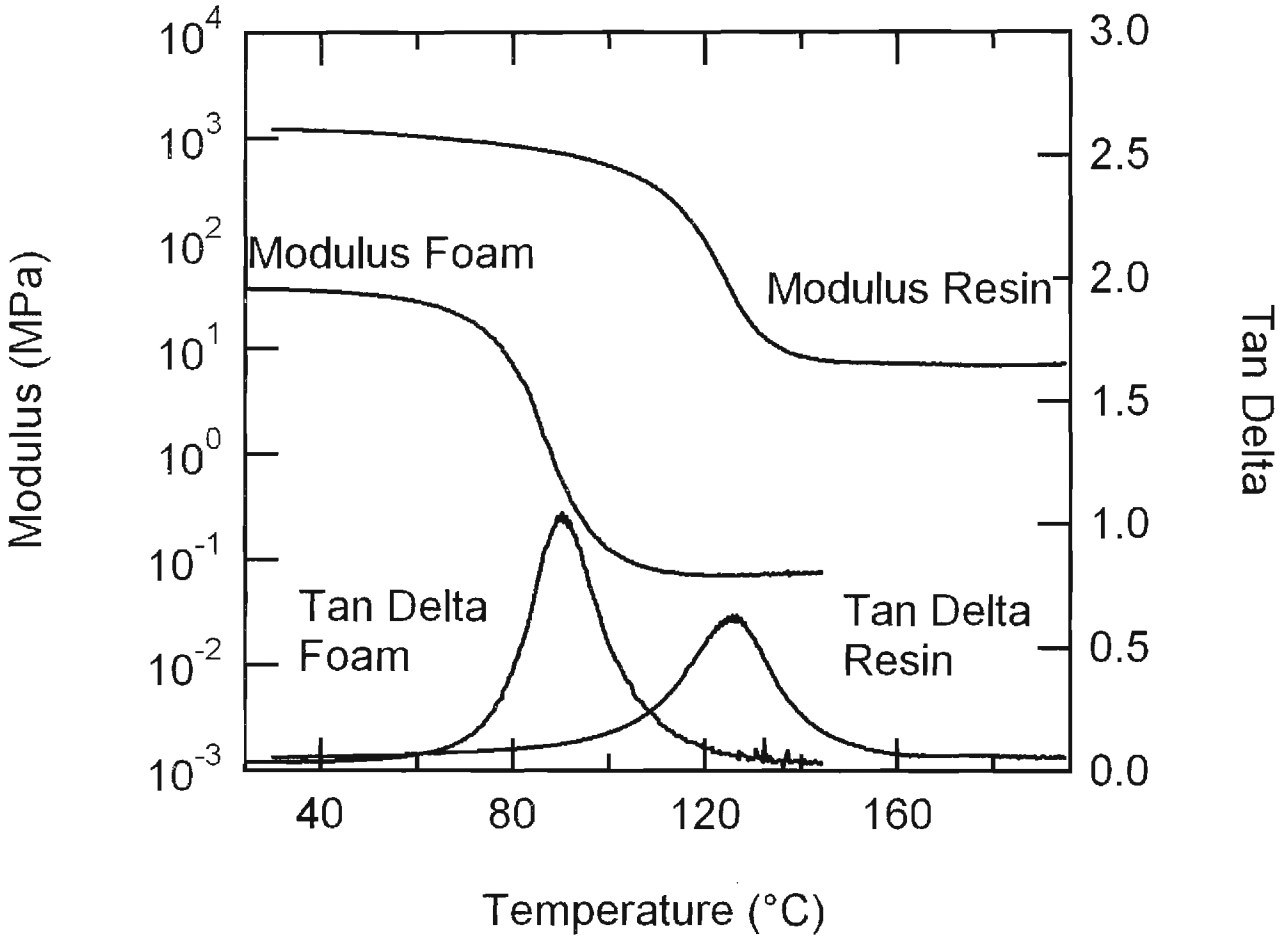
Modulus (MPa)
Tan Delta
Temperature (°C)
Modulus Foam
Modulus Resin
Tan Delta Foam
Tan Delta Resin
10^4
10^3
10^2
10^1
10^0
10^-1
10^-2
10^-3
3.0
2.5
2.0
1.5
1.0
0.5
0.0
40
80
120
160

**Figure 4:**

**a)**

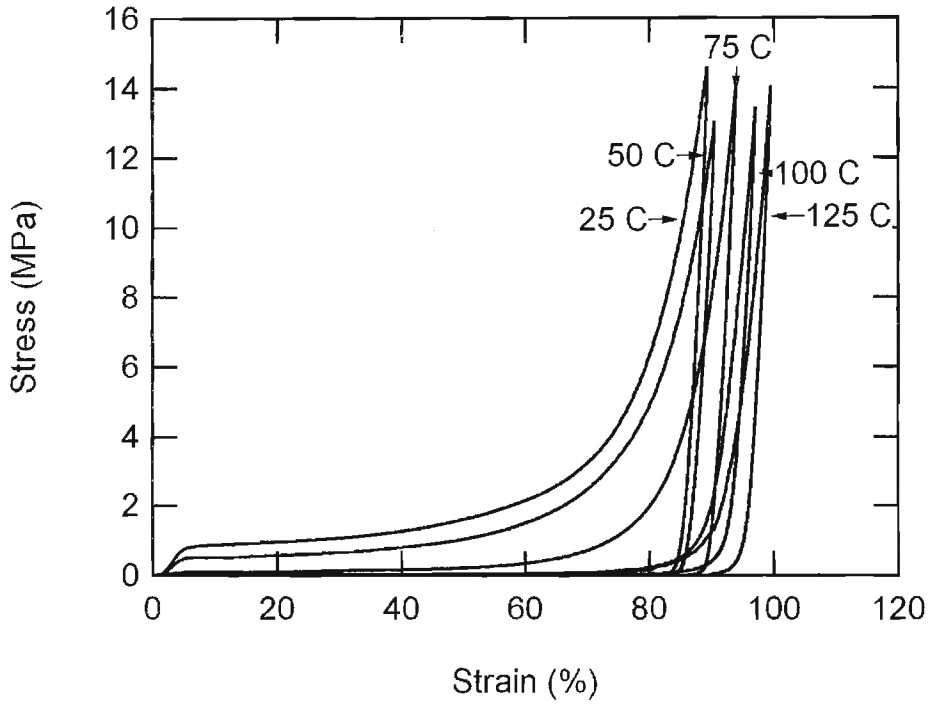
16
14
12
10
8
6
4
2
0
0
20
40
60
80
100
120
Stress (MPa)
Strain (%)
75 C
50 C
100 C
25 C
125 C

**b)**

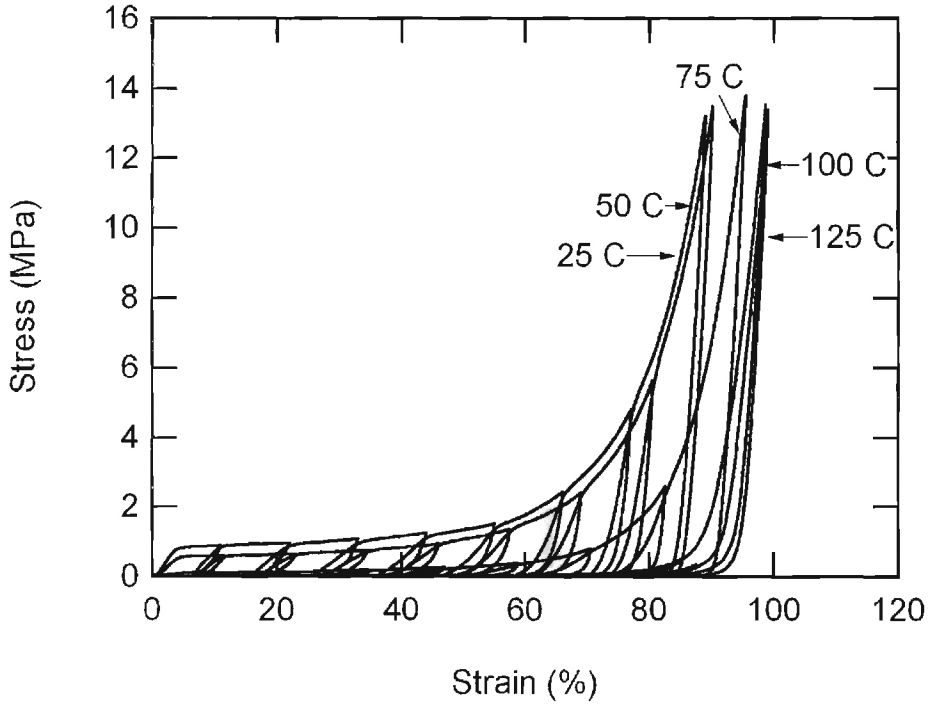
16
14
12
10
8
6
4
2
0
0
20
40
60
80
100
120
Stress (MPa)
Strain (%)
75 C
100 C
50 C
125 C
25 C

**c)**

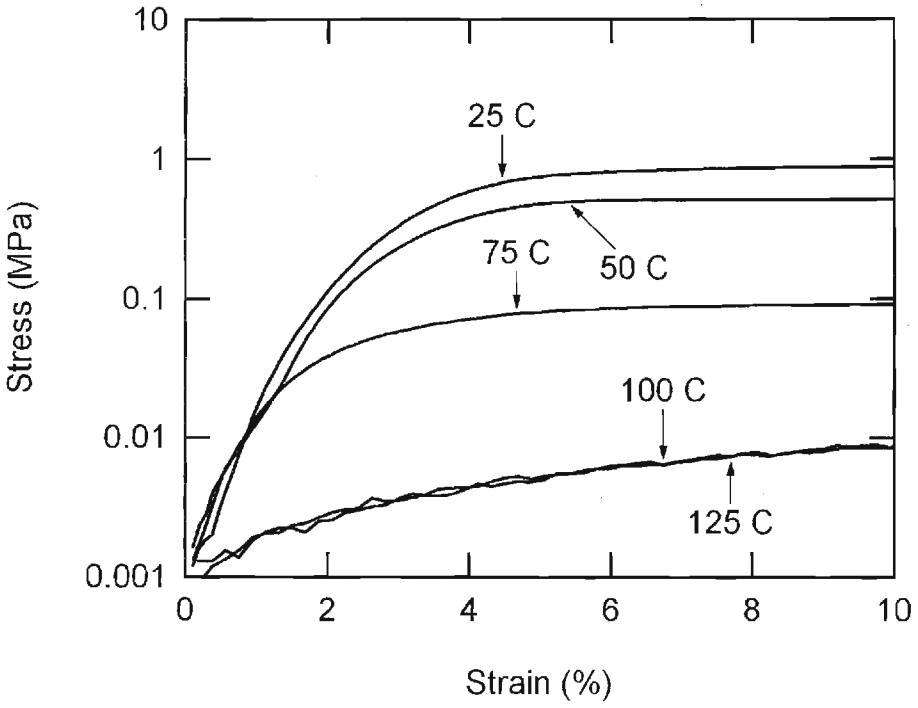
10
1
0.1
0.01
0.001
Stress (MPa)
25 C
75 C
50 C
100 C
125 C
0
2
4
6
8
10
Strain (%)

**Figure 5:**

a)

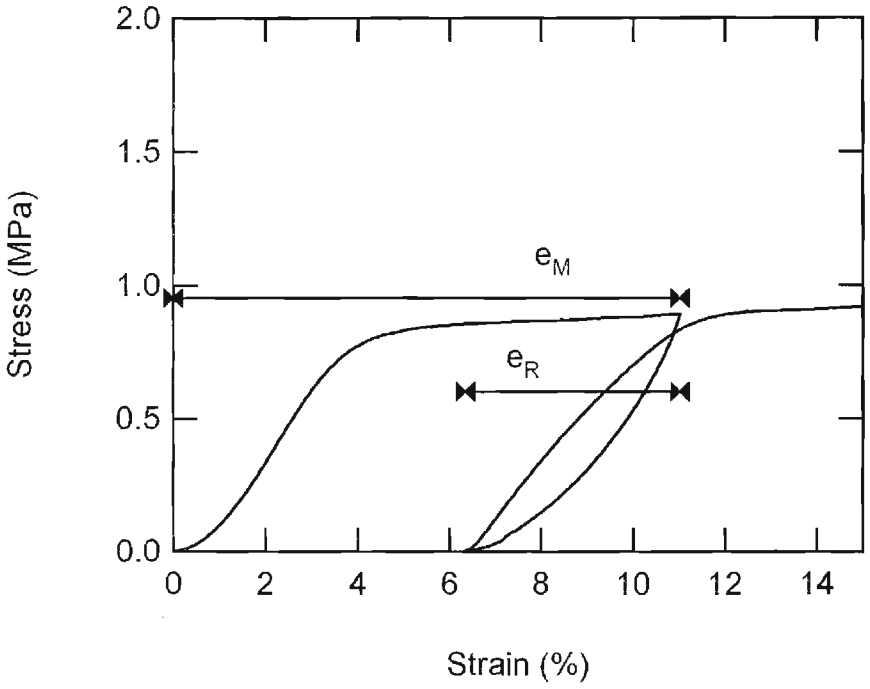
2.0
1.5
1.0
0.5
0.0
Stress (MPa)
$e_M$
$e_R$
0
2
4
6
8
10
12
14
Strain (%)

b)

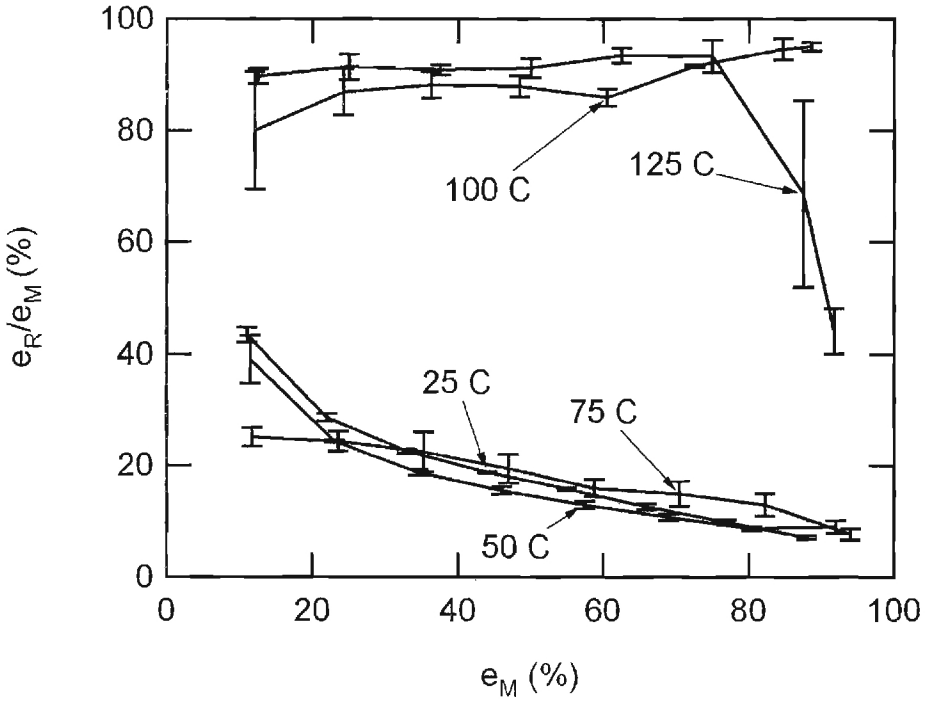
100
80
60
40
20
0
$e_R/e_M$ (%)
100 C
125 C
25 C
75 C
50 C
0
20
40
60
80
100
$e_M$ (%)

**Figure 6:**

**a)**

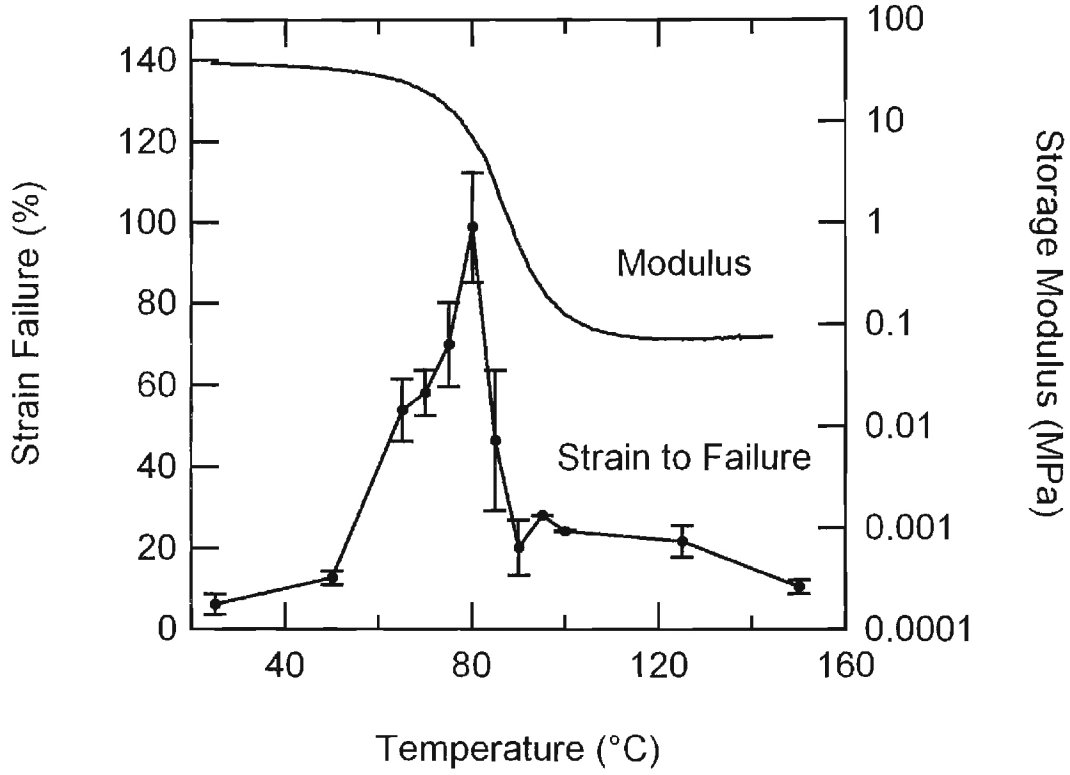
Strain Failure (%)
Storage Modulus (MPa)
Temperature (°C)
Modulus
Strain to Failure
140
120
100
80
60
40
20
0
100
10
1
0.1
0.01
0.001
0.0001
40
80
120
160

**b)**

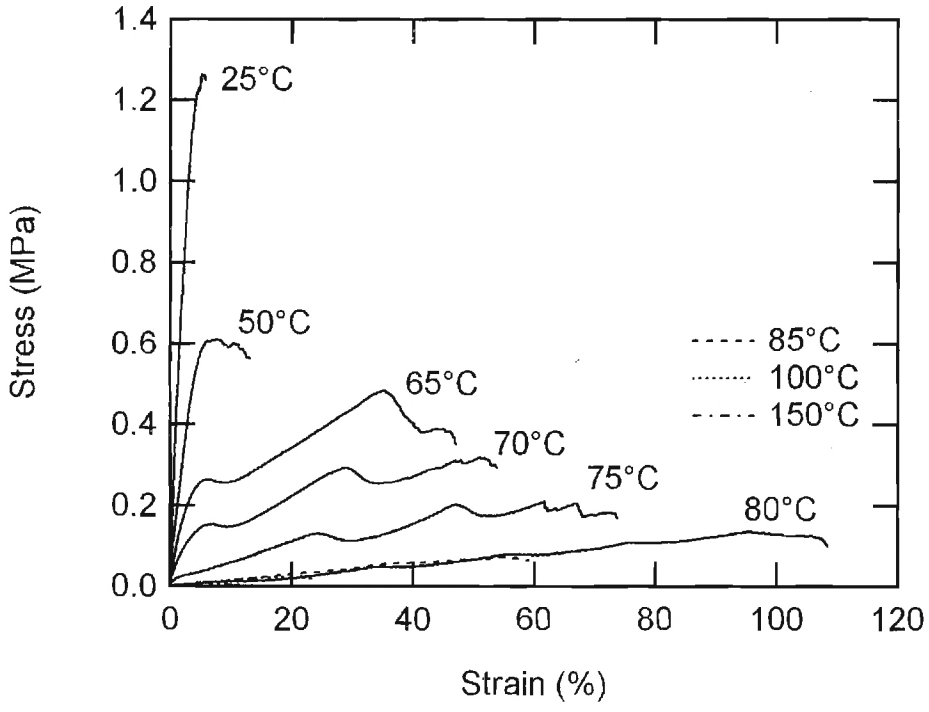
Stress (MPa)
Strain (%)
25°C
50°C
65°C
70°C
75°C
80°C
85°C
100°C
150°C
1.4
1.2
1.0
0.8
0.6
0.4
0.2
0.0
0
20
40
60
80
100
120

**Figure 7:**

**a)**

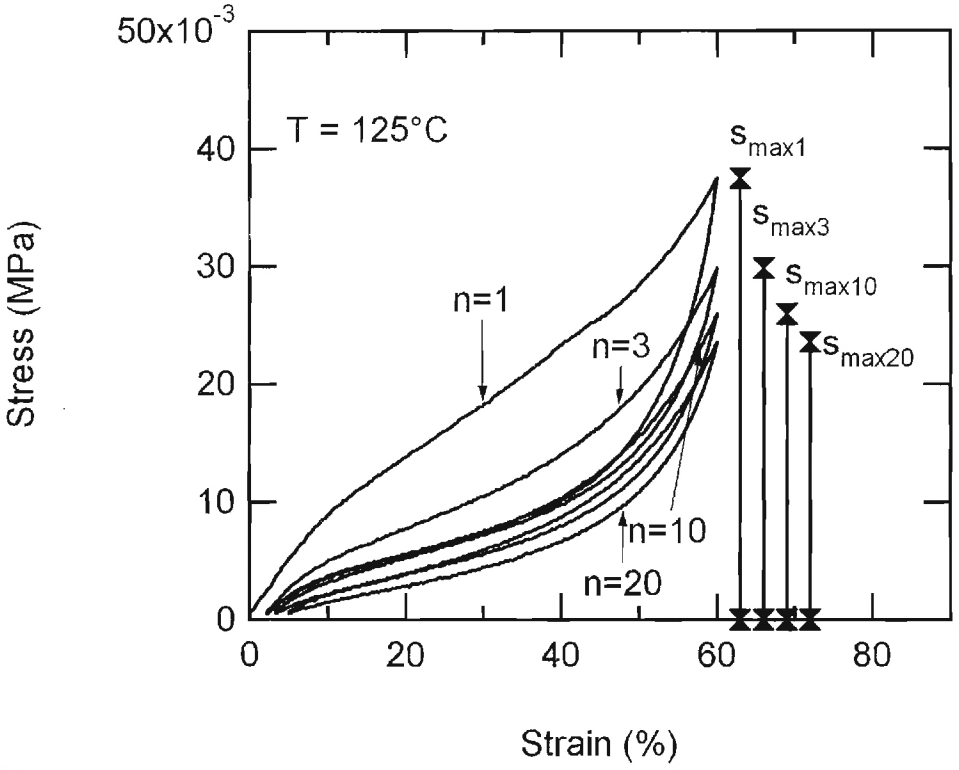
50x10-3
T = 125°C
smax1
smax3
smax10
smax20
n=1
n=3
n=10
n=20
Stress (MPa)
Strain (%)
0
10
20
30
40
0
20
40
60
80

**b)**

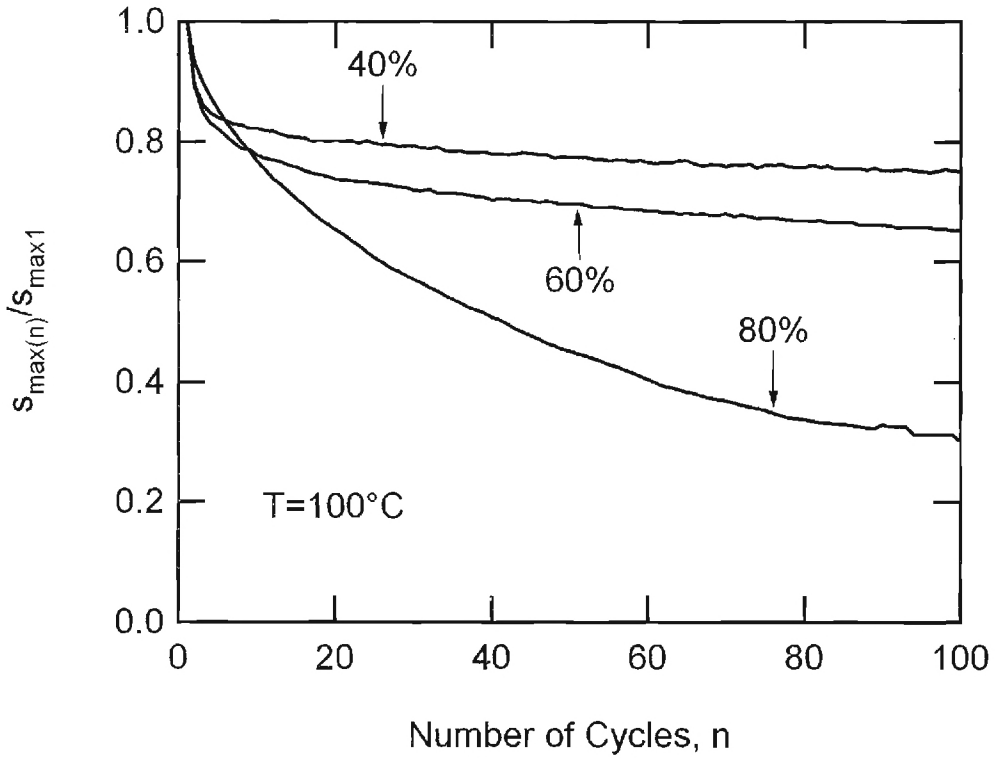
40%
60%
80%
T=100°C
smax(n)/smax1
Number of Cycles, n
0.0
0.2
0.4
0.6
0.8
1.0
0
20
40
60
80
100

c)

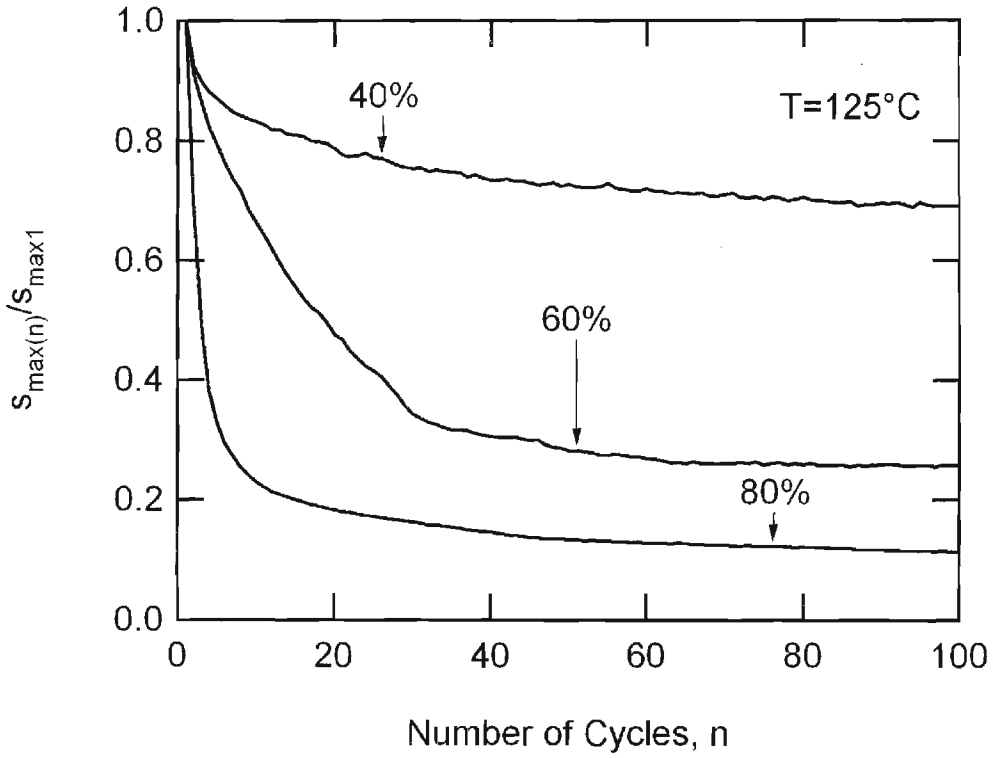
1.0
0.8
0.6
0.4
0.2
0.0
0
20
40
60
80
100
40%
60%
80%
T=125°C
$s_{max(n)}/s_{max1}$
Number of Cycles, n

**Figure 8:**

**a)**

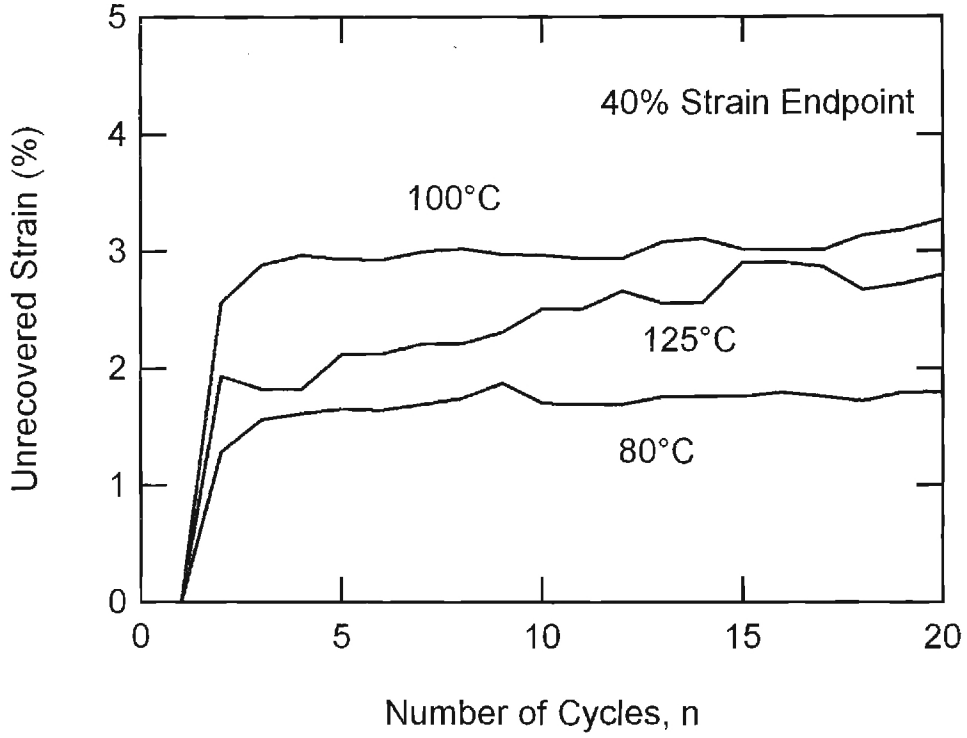
40% Strain Endpoint
100°C
125°C
80°C
Unrecovered Strain (%)
Number of Cycles, n
0
1
2
3
4
5
0
5
10
15
20

**b)**

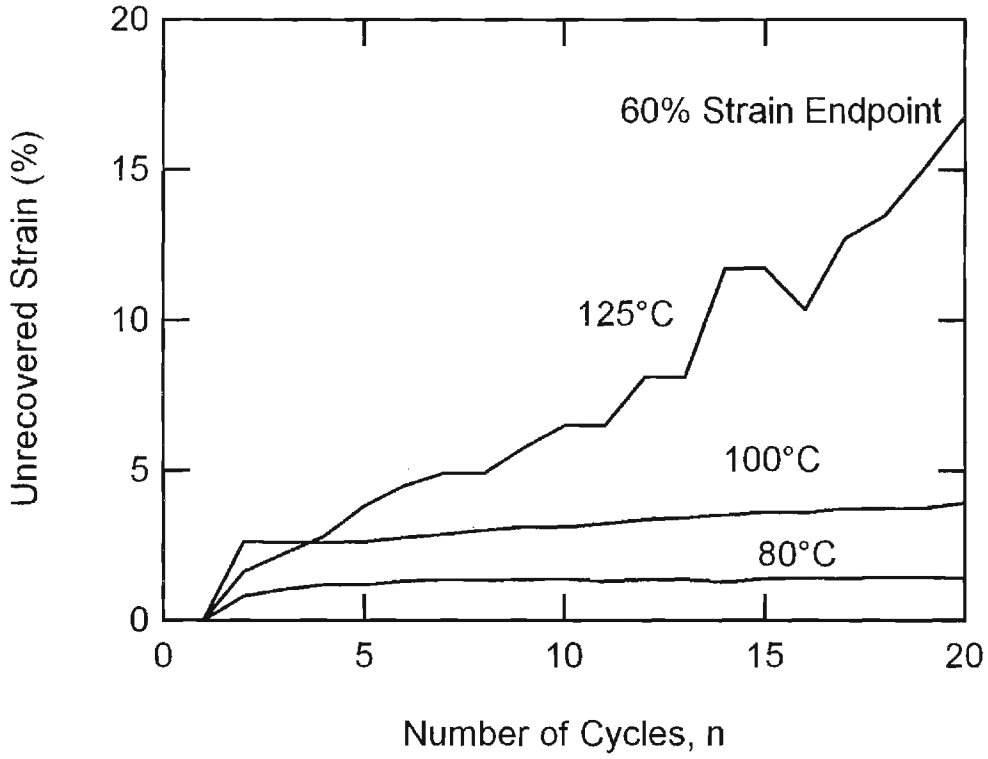
60% Strain Endpoint
125°C
100°C
80°C
Unrecovered Strain (%)
Number of Cycles, n
0
5
10
15
20
0
5
10
15
20

c)

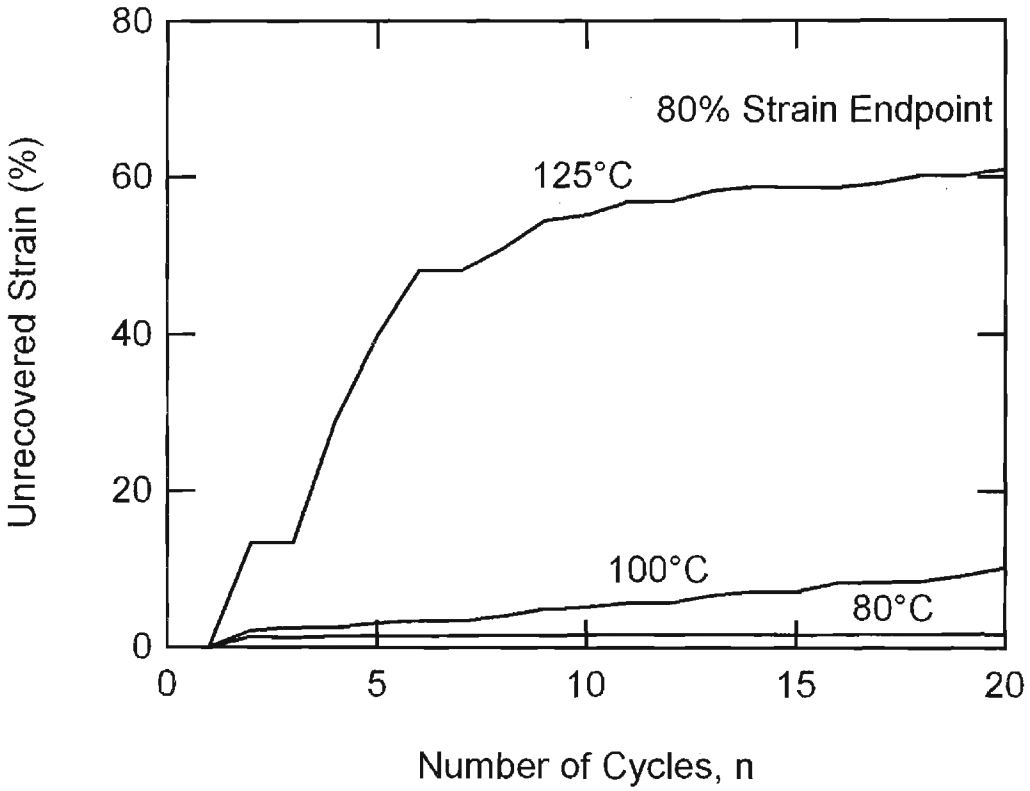
80
60
40
20
0
Unrecovered Strain (%)
80% Strain Endpoint
125°C
100°C
80°C
0
5
10
15
20
Number of Cycles, n

**Figure 9:**

a)

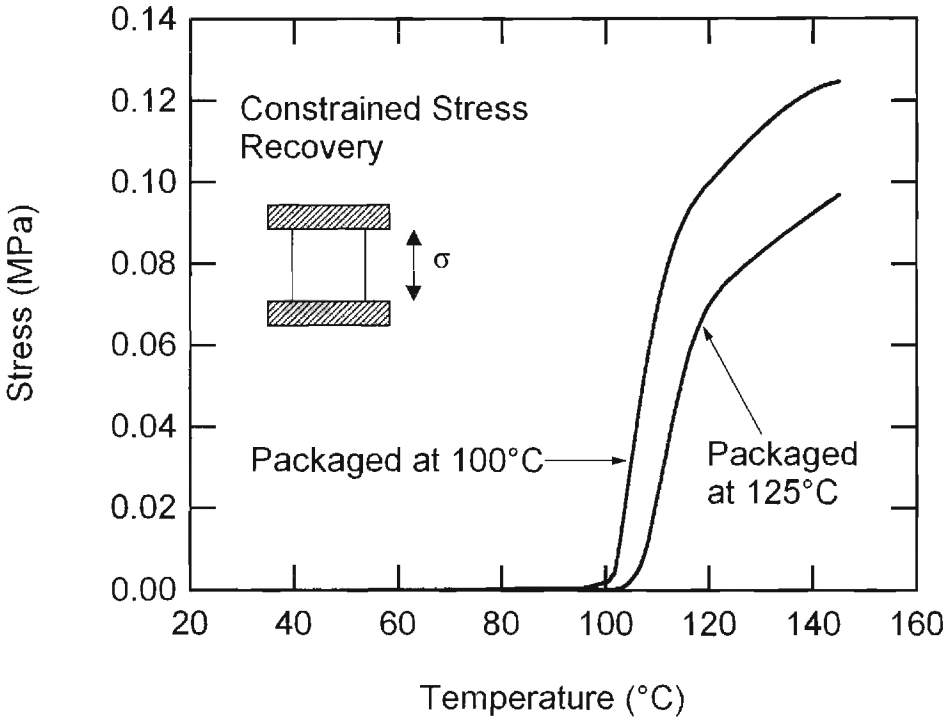
0.14
0.12
0.10
0.08
0.06
0.04
0.02
0.00
Stress (MPa)
Constrained Stress Recovery
σ
Packaged at 100°C
Packaged at 125°C
20
40
60
80
100
120
140
160
Temperature (°C)

b)

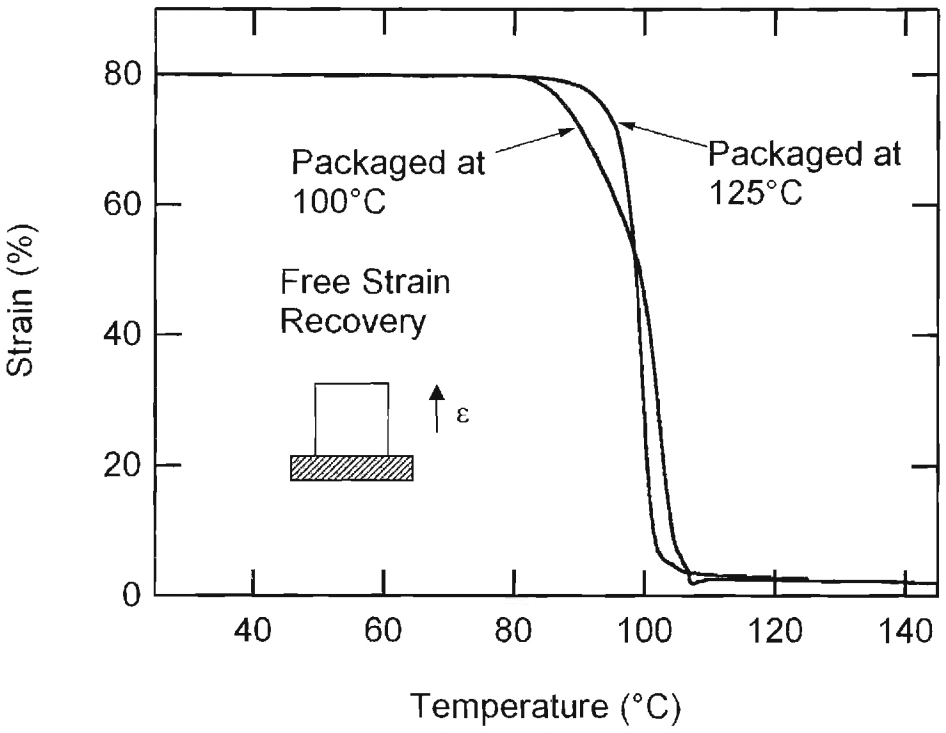
80
60
40
20
0
Strain (%)
Packaged at 100°C
Packaged at 125°C
Free Strain Recovery
ε
40
60
80
100
120
140
Temperature (°C)

**Figure 10:**

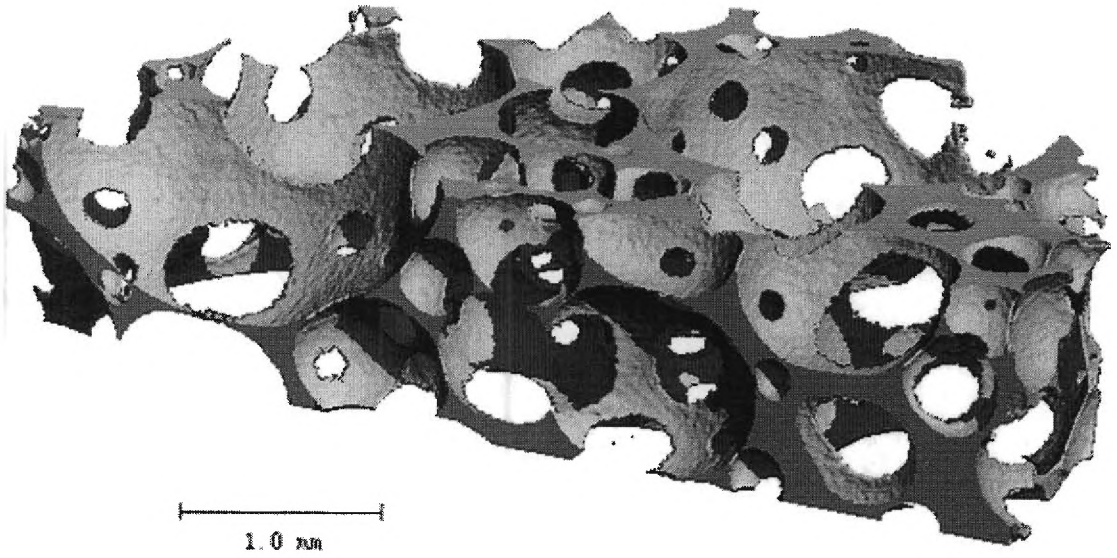

**Figure 11:**

**a)**

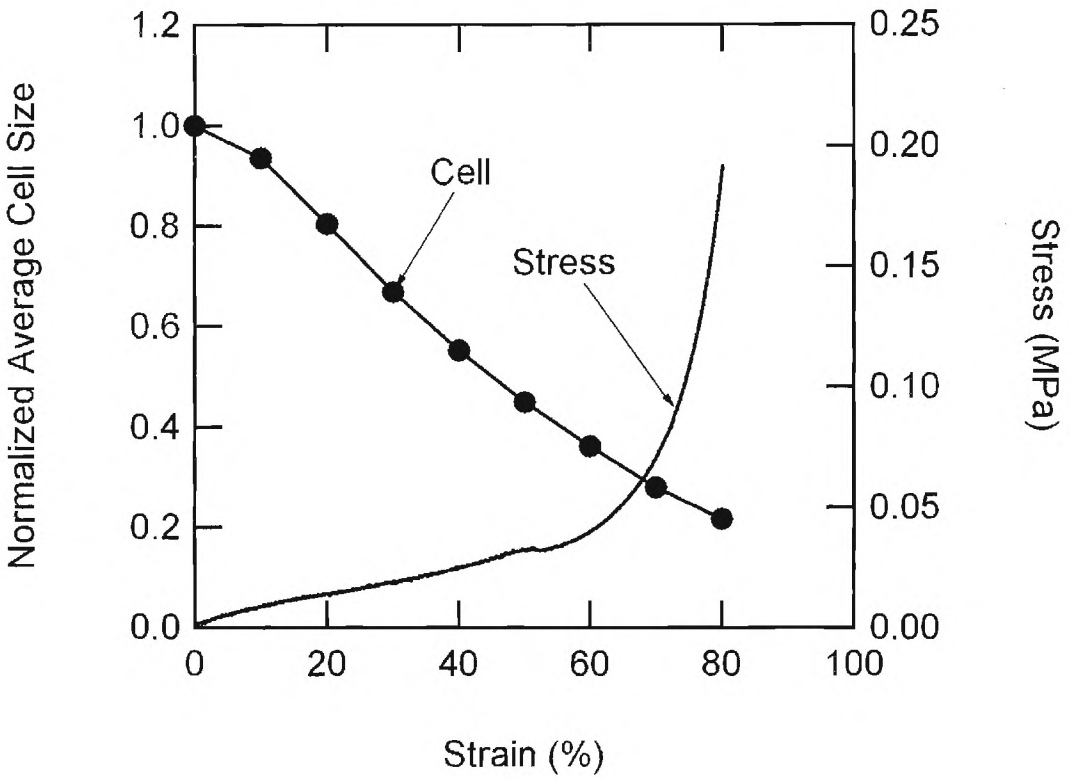
Normalized Average Cell Size
1.2
1.0
0.8
0.6
0.4
0.2
0.0
0.25
0.20
0.15
0.10
0.05
0.00
Stress (MPa)
Cell
Stress
0
20
40
60
80
100
Strain (%)

**b)**

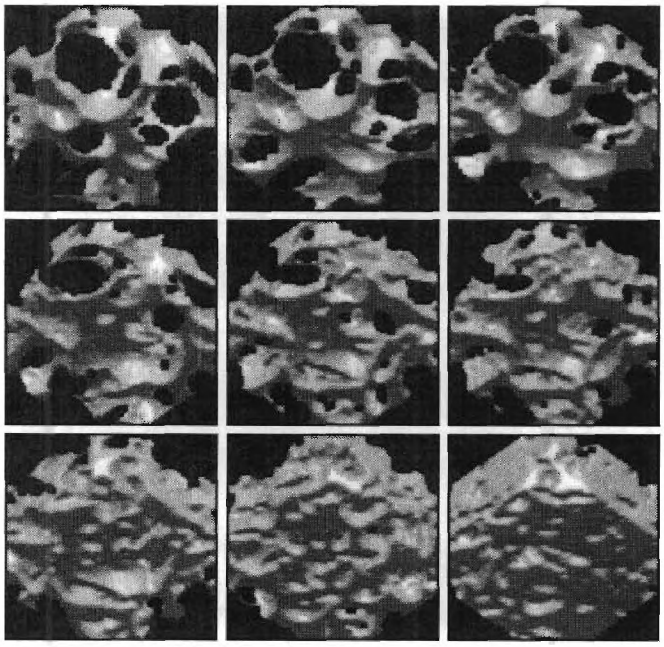

**c)**

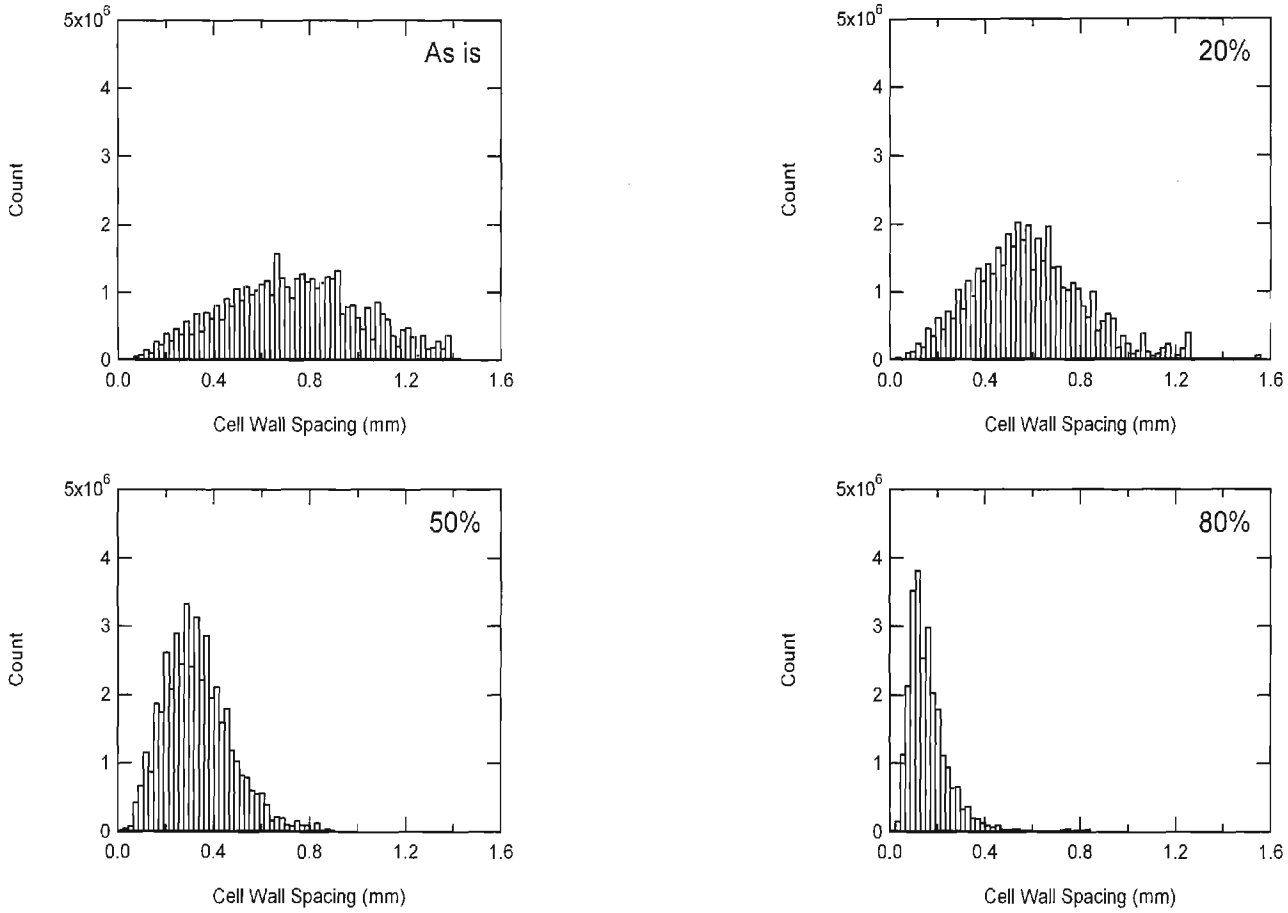
As is
20%
50%
80%
Count
Cell Wall Spacing (mm)
5x10^6
0
1
2
3
4
0.0
0.4
0.8
1.2
1.6

**Figure 1:** Shape memory storage process. The recovery step can also be used to package the material into another shape.

**Figure 2:** Cell response to compressive strain. In the elastic region the cell walls bend, from the yield point to the upswing ~60% strain, the cell walls buckle, and beyond buckling the cells wall make contact and densification begins.

**Figure 3:** Storage modulus and Tan Delta of the foam and resin from DMA tensile testing.

**Figure 4:** Engineering stress vs. engineering strain curves for varying temperatures (a) simple compression and (b) block compression (c) log scale of low strain region

**Figure 5:** Analysis of block compression testing (a) defining maximum strain, recovered strain, and loading profile while (b) a plot of recovered strain in terms of maximum strain
by maximum strain and temperature effect.

**Figure 6**: Tensile Failure peak (a) Average strain to failure versus various temperatures overlayed with storage modulus versus temperature (b) Select tensile curves at each temperature to show failure peak.

**Figure 7:** Effect of cycling on the maximum stress at a set strain. (a) Shows selected cycle curves and defines the maximum stress. (b) Effect at 100°C and (b) 125°C. The curves are labeled with the strain end point.

**Figure 8:** Temperature dependence on recovered strain during cyclic loading with varying strain endpoints; (a) 40% compressed, (b) 60% compressed, and (c) 80% compressed.

**Figure 9:** Shape recovery properties at packaging temperatures 100°C and 125°C (a) constrained stress recovery and (b) free strain recovery.

**Figure 10:** 6μm resolution x-ray micro-CT image of as received foam. The cells appear to be spherical and uniformly distributed through out the foam.

**Figure 11**: Micro-structural response to deformation at 125°C. (a) Plot of average cell size versus strain, stress-strain plot is included for comparison. (b) Snap shot of the same 2x2x0.8 mm foam region during deformation at 10% strain intervals. Reads left to right, top to bottom starting at un-deformed and ending at 70% compressed. (c) Selected histograms of cell wall spacing vs. count number of the foam as its being deformed.